Electronic Supplementary Material (ESI) for Physical Chemistry Chemical Physics.

Electron injection effect in In_2O_3 and SnO_2 nanocrystals modified by ruthenium heteroleptic complexes

Sergey Tokarev, Marina Rumyantseva, Abulkosim Nasriddinov, Alexander Gaskov, Anna Moiseeva, Yuri Fedorov, Olga Fedorova, Gediminas Jonusauskas

SUPPORTING INFORMATION

Contents

Experimental 2

- Synthesis of ligands, general procedure 2
- Synthesis of complexes, general procedure 2
- Synthesis of bis(2,2'-bipyridin-k^{2}N^1,N$^{1'}$)[2-2,2'-bithiophen-5-yl)-1H-imidazo[4,5-f][1,10]phenanthroline-k^{2}N^7,N^8]ruthenium dichloride (8) 3
- NMR Spectra of bis(2,2'-bipyridin-k^{2}N^1,N$^{1'}$)[2-2,2'-bithiophen-5-yl)-1H-imidazo[4,5-f][1,10]phenanthroline-k^{2}N^7,N^8]ruthenium dichloride (8) 4

Photophysical properties 6

- Emission decay curves for solutions 8
- Emission decay curves for hybrid materials 10
- Electrochemistry studies 14

References: 16

Experimental

Benzaldehyde, 4-(dimethylamino)benzaldehyde, thiophene-2-carbaldehyde, 2,2'-bithiophene-5-carbaldehyde, potassium bromate, sulfuric acid, ammonium acetate, glacial acetic acid, *cis*-bis(2,2-bipyridine)dichlororuthenium (II) hydrate, tetrabutylammonium perchlorate (TBAP) (Fluka) were commercially available and were used without further purification. Phenantoline-5,6-dione and 1,4-dimethylpyridin-1-ium iodide were prepared as described elsewhere [1,2] respectively. Anhydrous acetonitrile (MeCN) and dimethylformamide (DMF) for electrochemical measurements were electronic grade purity and were used as received. Spectroscopic grade MeCN was used for recording of the absorption spectra.

^{1}H and ^{13}C (APT method) NMR spectra were recorded on a Bruker AVANCE-400 and Avance-500 spectrometers. The chemical shifts and spin-spin coupling constants were determined with accuracy of 0.01 ppm and 0.1 Hz, respectively. Two-dimensional techniques HMQC, HMBC and COSY were used for the assignment of signals in the spectra.

LDI-TOF mass spectra were collected with Bruker Autoflex II instrument, samples were irradiated with nitrogen laser (l = 337 nm). Isotopic patterns were calculated with IsotopeViewer 2000.

Elemental analysis was performed in the A.N. Nesmeyanov Institute of Organoelement Compounds of Russian Academy of Sciences.

Synthesis of ligands, general procedure

Synthesis of 2-substituted-1H-imidazo[4,5-f][1,10]phenantrolines **1-4** were carried out as described in [3]. The synthetic procedure includes the condensation of phenathroline-5,6-dione with corresponding aldehyde in a solution of glacial acetic acid in the presence of ammonium acetate for 4-8 hours at reflux. After the reaction was completed an aqueous solution of NH_4OH was added to pH ~ 8. The precipitate formed was filtered on a glass porous filter, washed with water and diethyl ether. The physicochemical characteristics of the compounds **1-4** are described in [4] (**3,4**) [5] (**1**) [6] (**2**).

Synthesis of complexes, general procedure

Synthesis of heteroleptic complexes **5-8** were carried out as described earlier [7] A solution of the corresponding 1H-imidazo [4,5-f] [1,10] phenanthroline derivative and *cis*-bis(2,2-bipyridine)dichlororuthenium (II) hydrate in absolute ethanol was placed in a tube, degassed 3 times and filled with argon. The tube was sealed and kept at 80°C for 8 hours. Next, the tube was opened and the solvent was evaporated on a rotary evaporator. The resulting crude product was purified by column chromatography on alumina, eluent – a mixture of benzene:methanol in a ratio of 10:1. The physicochemical characteristics of the compounds **5-7** are described in [8] (**5**) [9] (**6**) [10] (**7**). The structure of novel compound **8** was confirmed by ^{1}H, ^{13}C NMR spectroscopy, elemental analysis and mass-spectrometry methods (Figs. S2-S6 in Supporting Information (SI))

Synthesis of bis(2,2’-bipyridin-k^{2}N^1,N$^{1’}$)[2-2,2’-bithiophen-5-yl)-1H-imidazo[4,5-f][1,10]phenanthroline-k^{2}N^7,N^8]ruthenium dichloride (8)

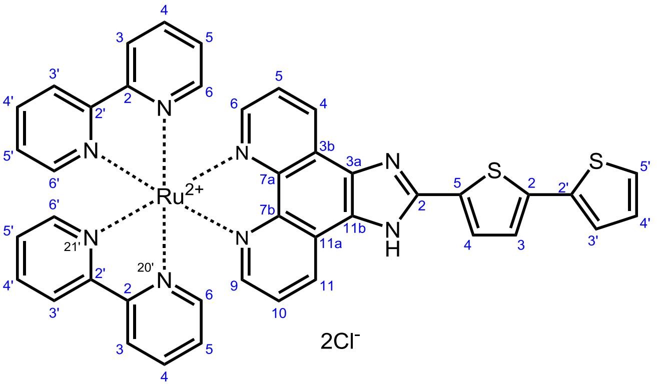

Figure S1. Structure of the bis(2,2’-bipyridin-k^{2}N^1,N$^{1’}$)[2-2,2’-bithiophen-5-yl)-1H-imidazo[4,5-f][1,10]phenanthroline-k^{2}N^7,N^8]ruthenium dichloride.

Following the general procedure, from 2-(2,2'-bithiophen-5-yl)-1H-imidazo[4,5-f][1,10] phenanthroline (**4**) (0.21 mmol, 80 mg) and *cis*-bis(2,2-bipyridine)dichlororuthenium (II) hydrate (0.21 mmol, 100 mg) in 6.5 ml of absolute ethanol 74 mg of an orange precipitate were obtained after the purification by column chromatography (benzene : methanol=10:1 on alumina) The yield is 41%.

^{1}H NMR (methanol-d4, δ; ppm, J/Hz): 7.08 (t, 1H, ^{3}J = 4.3, Th(4’)), 7.22 (d, 1H, ^{3}J = 3.8, Th(3')), 7.26 (d, 1H, ^{3}J =3.5, Th(3)), 7.37 (m, 3H, Th(5’), bpy(5’)), 7.57 (t, 2H, ^{3}J =6.6, bpy(5)), 7.71 (dd, 2H, ^{3}J = 5.3, ^{3}J = 8.2, ImPh(5,10)), 7.74 (d, 2H, ^{3}J =5.7, bpy(6’)), 7,81 (d, 1H, ^{3}J =3.7, Th(4)), 7.97 (m, 4H, ImPh(6,9), bpy(6)), 8.07 (t, 2H, ^{3}J =7.9, bpy(4’)), 8.18 (t, 2H, ^{3}J =7.9, bpy(4)), 8.74 (d, 2H, ^{3}J =8.1, bpy(3')), 8.77 (d, 2H, ^{3}J =8,2, bpy(3)), 8.99 (d, 2H, ^{3}J =8.2, ImPh(4,11)).

^{13}C NMR APT (methanol-d4, δ; ppm): [CH]: 123.63 (Th(3’)), 123.99 (Th (3)), 124.07 (bpy(3’)), 124.12 (bpy(3)), 124.61 (Th(5’)), 124.90 (ImPh(5,10)), 126.21 (Th(4)), 127.39 (bpy(5’)), 127.41 (bpy(5)), 127.70 (Th(4’)), 130.25 (ImPh(4,11)), 137.53 (bpy(4’)), 137.65 (bpy(4)), 147.84 (ImPh(6,9)), 151.30 (bpy(6’)), 151.36 (bpy(6)). [C]: 125.00 (ImPh(3b,11a)), 135.33 (Th(5)), 135.94 (ImPh(3a,11b)), 136.77 (Th(2’)), 138.05 (Th(2)), 144.60 (ImPh(7a,7b)), 154.01 (ImPh(2)), 157.16 (bpy(2’)), 157.40 (bpy(2)).

MALDI-MS m/z: 398.3 [M-2Cl]$^{2+}$.

Calculated for $C_{41}H_{28}Cl_2N_8RuS_2$ (%): C, 56.68; H, 3.25; N, 12.90; Ru, 11.63, found (%): C, 56.78 H, 3.24; N, 12.98; Ru, 11.56.

NMR Spectra of bis(2,2'-bipyridin-k^{2}N^1,N$^{1'}$)[2-2,2'-bithiophen-5-yl)-1H-imidazo[4,5-f][1,10]phenanthroline-k^{2}N^7,N^8]ruthenium dichloride (8)

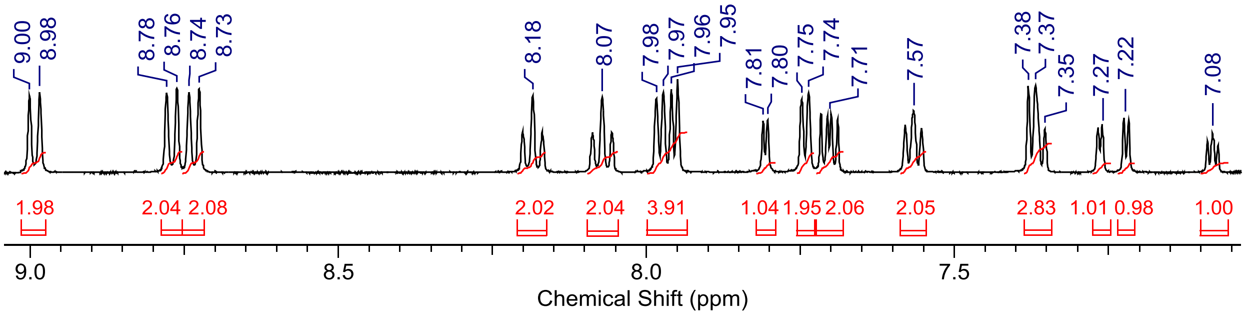

Figure S2. ^{1}H NMR-spectra of **8** in CD_3OD, Bruker 400 MHz

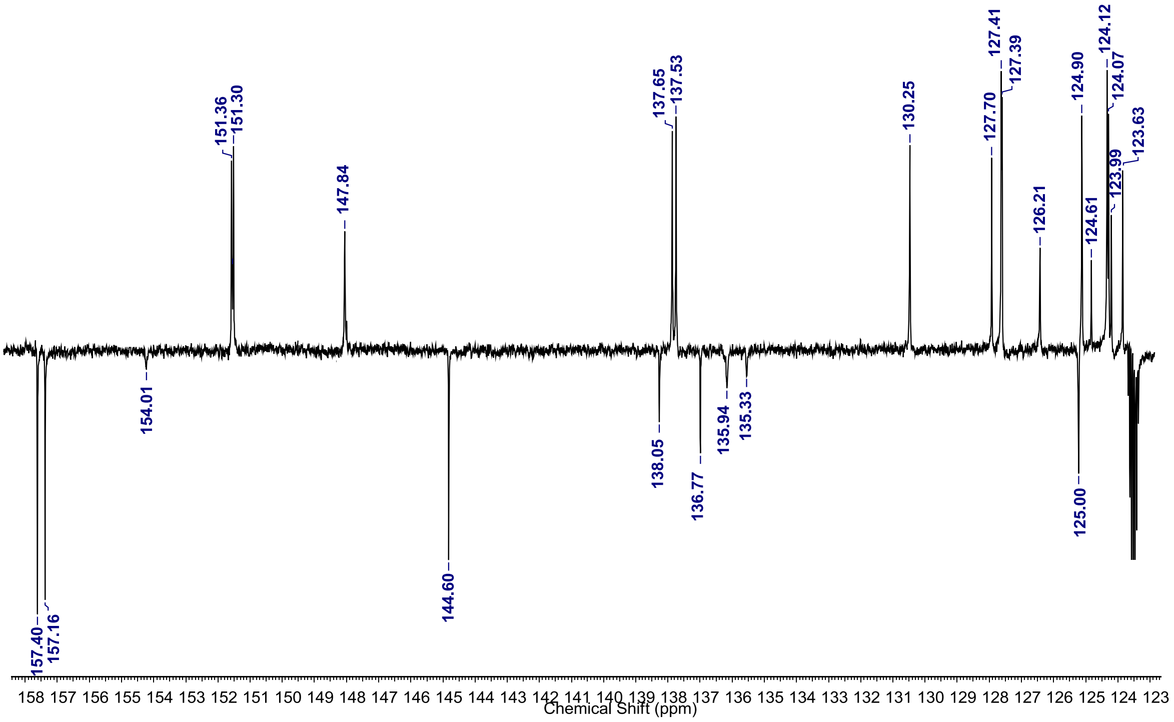

Figure S3. ^{13}C NMR-spectra of **8** in CD_3OD, Bruker 400 MHz

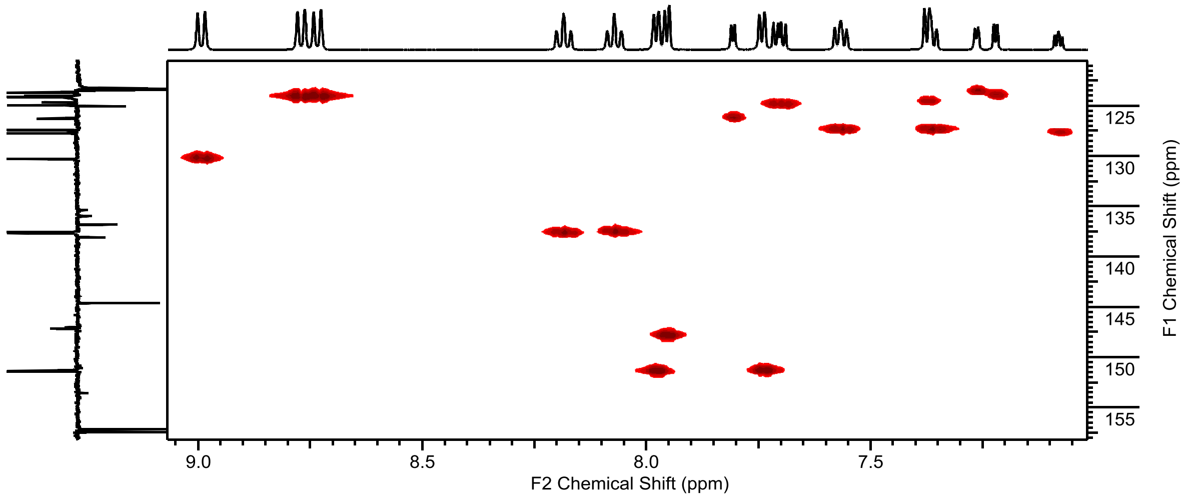

Figure S4. HMQC NMR-spectra of **8** in CD_3OD, Bruker 400 MHz

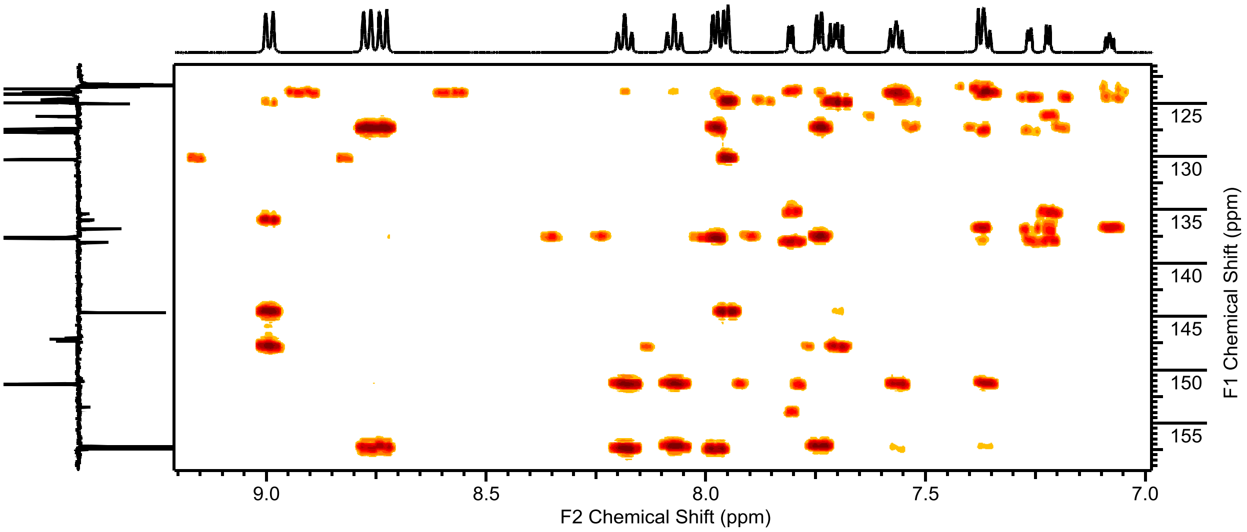

Figure S5. HMBC NMR-spectra of **8** in CD$_3$OD, Bruker 400 MHz

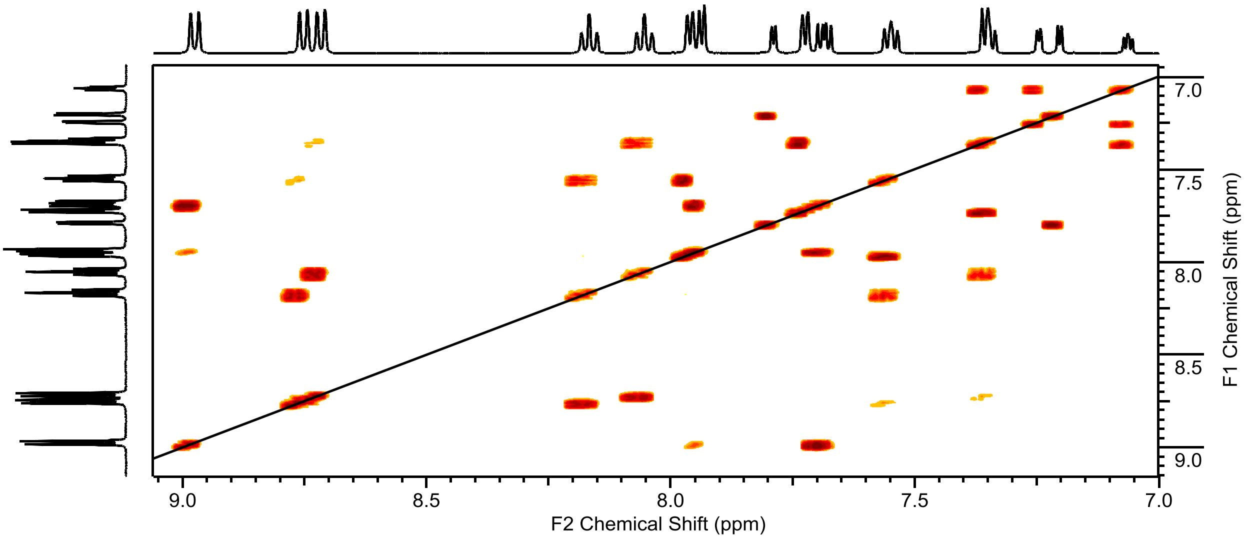

Figure S6. COSY NMR-spectra of **8** in CD$_3$OD, Bruker 400 MHz

---

Photophysical properties

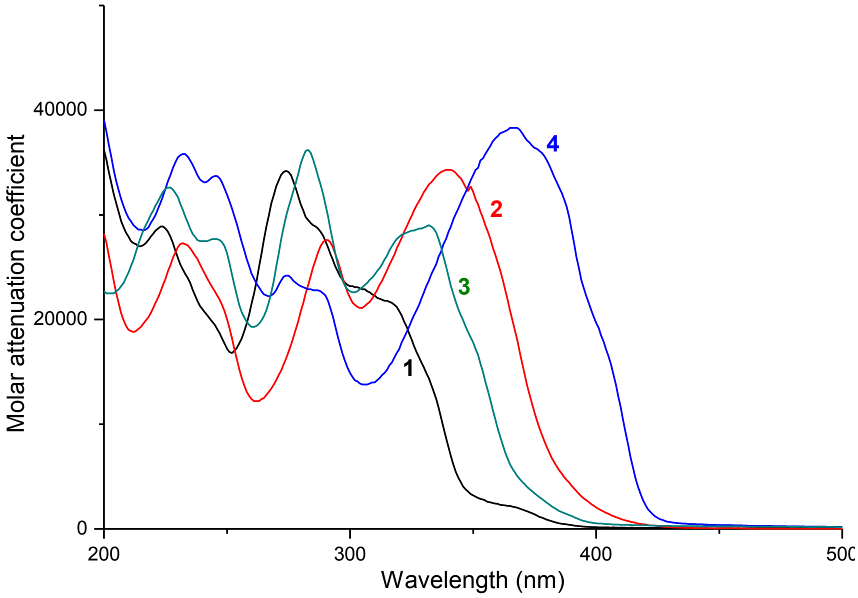

Figure S7. Electronic absorption spectra of **1-4** in acetonitrile, $C_{\mathbf{6\text{-}10}}=2*10^{-5}$ M.

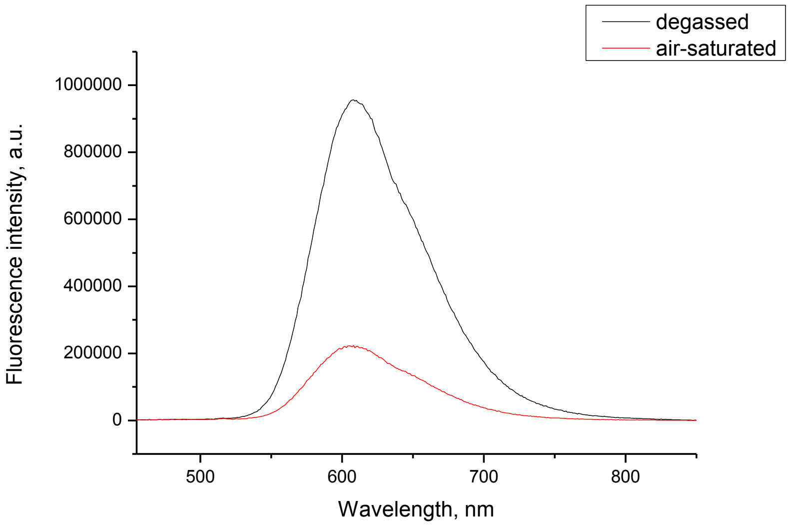

Figure S8. Normalized emission spectrum of **5** in methanol, λ_{ex} = 450 nm.

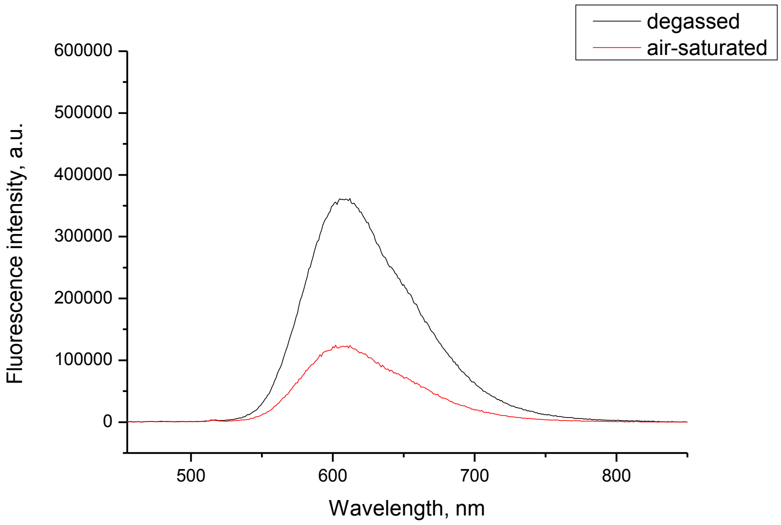

Figure S9. Normalized emission spectrum of **6** in methanol, λ_{ex} = 450 nm.

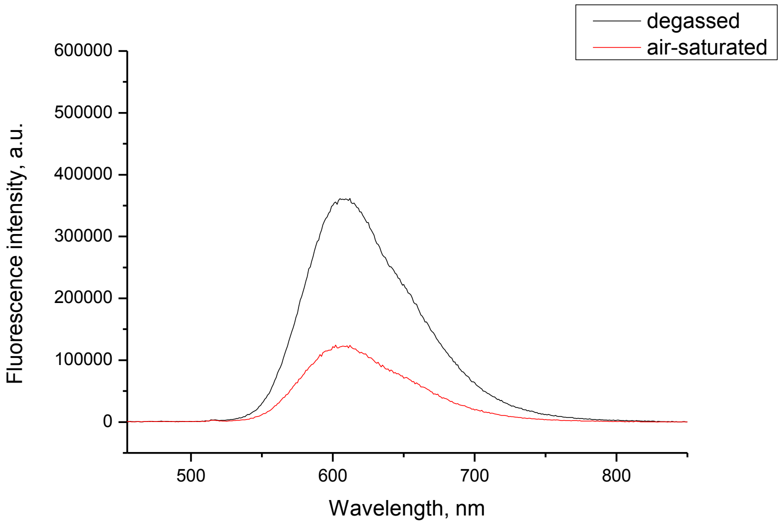

Figure S10. Normalized emission spectrum of **7** in methanol, λ_{ex} = 450 nm.

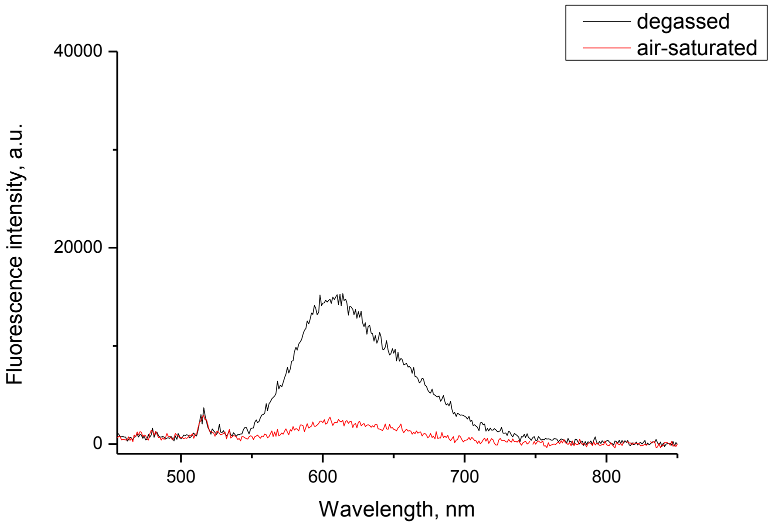

Figure S11. Normalized emission spectrum of **8** in methanol, λ_{ex} = 450 nm.

Emission decay curves for solutions

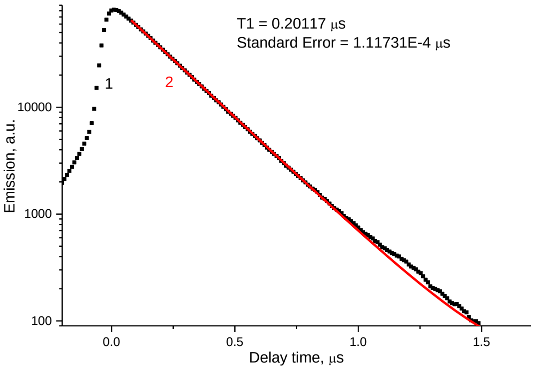

Figure S12. Time-resolved decay of **5** emission (λ_{exc} = 450 nm, emission range: 550-700 nm, 1, black) in air-saturated methanol, and the best monoexponential fit of luminescence decay (2, red) in log scale. T1 – luminescence lifetime.

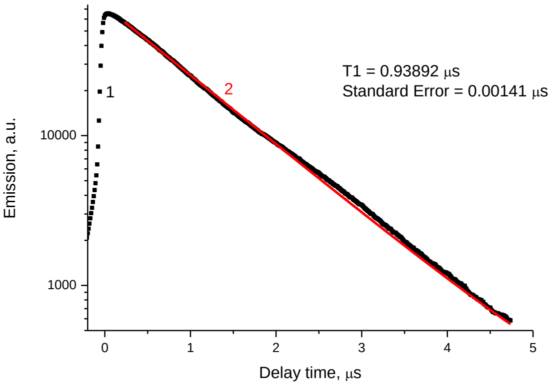

Figure S13. Time-resolved decay of **5** emission (λ_{exc} = 450 nm, emission range: 550-700 nm, 1, black) in degassed methanol, and the best monoexponential fit of luminescence decay (2, red) in log scale. T1 – luminescence lifetime.

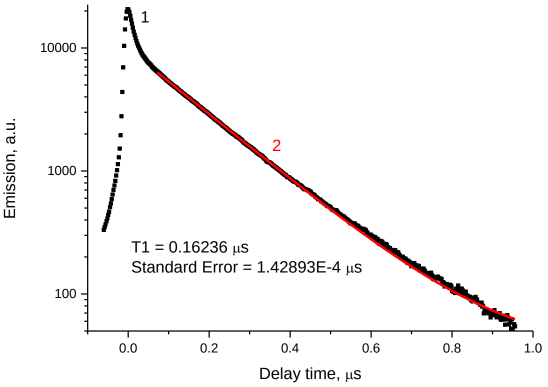

Figure S14. Time-resolved decay of **6** emission (λ_{exc} = 450 nm, emission range: 550-700 nm, 1, black) in air-saturated methanol, and the best monoexponential fit of luminescence decay (2, red) in log scale. T1 – luminescence lifetime.

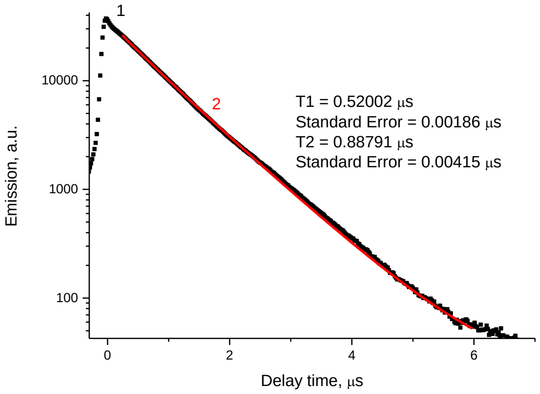

Figure S15. Time-resolved decay of **6** emission (λ_{exc} = 450 nm, emission range: 550-700 nm, 1, black) in degassed methanol, and the best biexponential fit of luminescence decay (2, red) in log scale. T1, T2 – luminescence lifetimes.

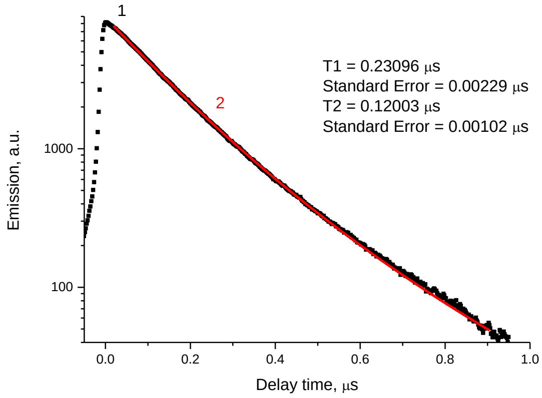

Figure S16. Time-resolved decay of **7** emission (λ_{exc} = 450 nm, emission range: 550-700 nm, 1, black) in air-saturated methanol, and the best biexponential fit of luminescence decay (2, red) in log scale. T1, T2 – luminescence lifetimes.

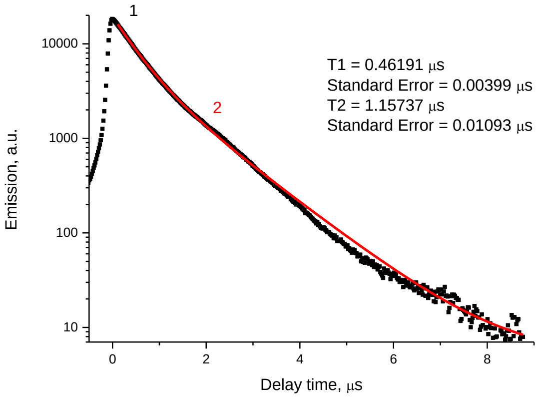

Figure S17. Time-resolved decay of **7** emission (λ_{exc} = 450 nm, emission range: 550-700 nm, 1, black) in degassed methanol, and the best biexponential fit of luminescence decay (2, red) in log scale. T1, T2 – luminescence lifetimes.

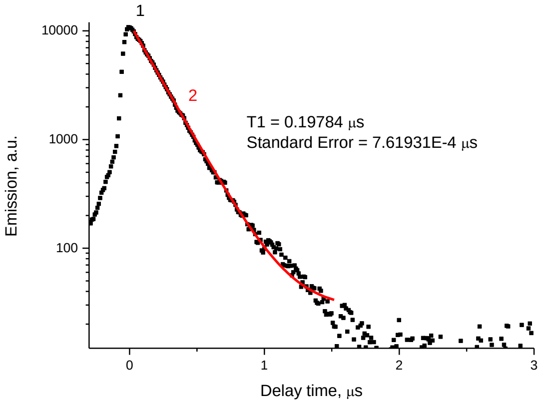

Figure S18. Time-resolved decay of **8** emission (λ_{exc} = 450 nm, emission range: 550-700 nm, 1, black) in air-saturated methanol, and the best monoexponential fit of luminescence decay (2, red) in log scale. T1 – luminescence lifetime.

Emission decay curves for hybrid materials

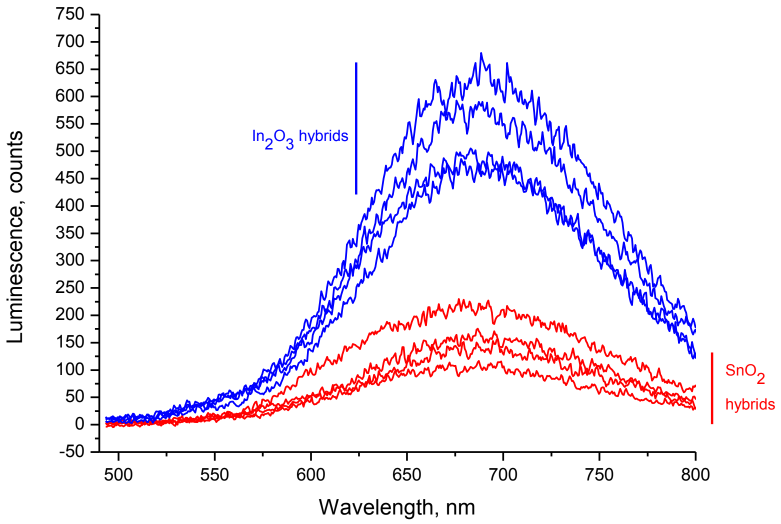

Figure S19. Spectra of red-shifted components of different hybrid materials based on In_2O_3 (blue) and SnO_2 (red) obtained from the luminescence decay maps by integrating the intensity over wavelengths in the period of 1.5–5 μs, when the short-lived luminescence has already ended

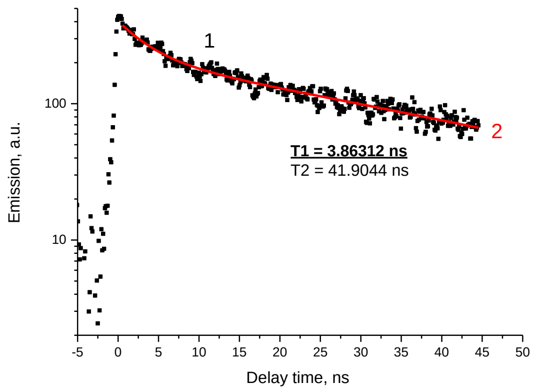

Figure S20. Time-resolved decay of emission of hybrid material **5**-In_2O_3 (λ_{exc} = 460 nm, emission range: 560-620 nm, 1, black) in the air, and the best biexponential fit of luminescence decay (2, red) in log scale. T1, T2 – luminescence lifetimes.

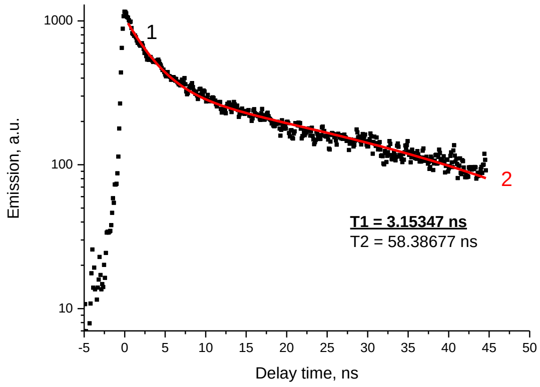

Figure S21. Time-resolved decay of emission of hybrid material **5**-SnO_2 (λ_{exc} = 460 nm, emission range: 560-620 nm, 1, black) in the air, and the best biexponential fit of luminescence decay (2, red) in log scale. T1, T2 – luminescence lifetimes.

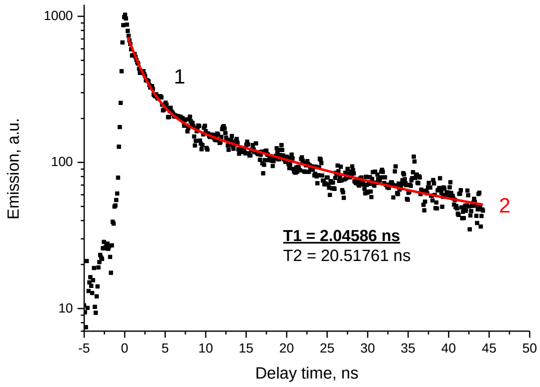

Figure S22. Time-resolved decay of emission of hybrid material **6**-In_2O_3 (λ_{exc} = 460 nm, emission range: 560-620 nm, 1, black) in the air, and the best biexponential fit of luminescence decay (2, red) in log scale. T1, T2 – luminescence lifetimes.

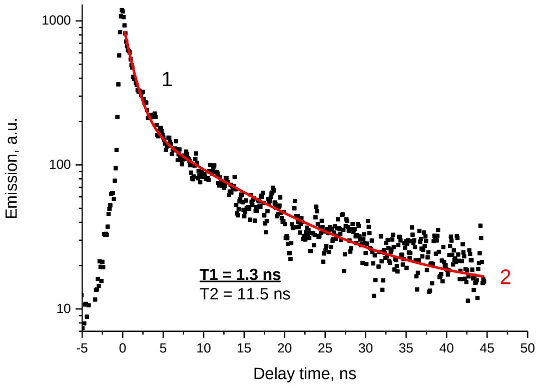

Figure S23. Time-resolved decay of emission of hybrid material **6**-SnO_2 (λ_{exc} = 460 nm, emission range: 560-620 nm, 1, black) in the air, and the best biexponential fit of luminescence decay (2, red) in log scale. T1, T2 – luminescence lifetimes.

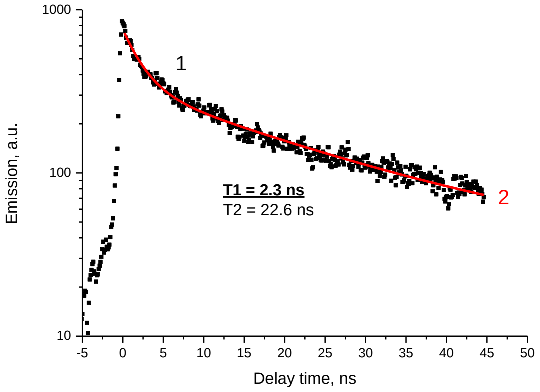

Figure S24. Time-resolved decay of emission of hybrid material **7**-In_2O_3 (λ_{exc} = 460 nm, emission range: 560-620 nm, 1, black) in the air, and the best biexponential fit of luminescence decay (2, red) in log scale. T1, T2 – luminescence lifetimes.

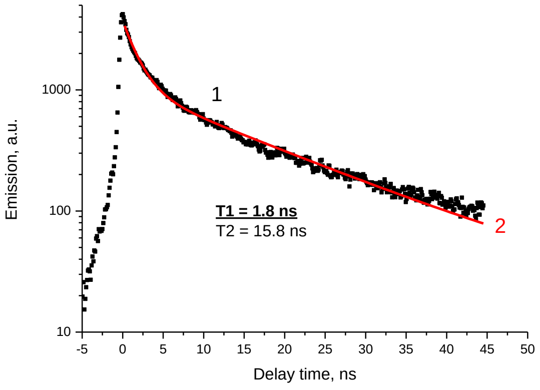

Figure S25. Time-resolved decay of emission of hybrid material **7**-SnO_2 (λ_{exc} = 460 nm, emission range: 560-620 nm, 1, black) in the air, and the best biexponential fit of luminescence decay (2, red) in log scale. T1, T2 – luminescence lifetimes.

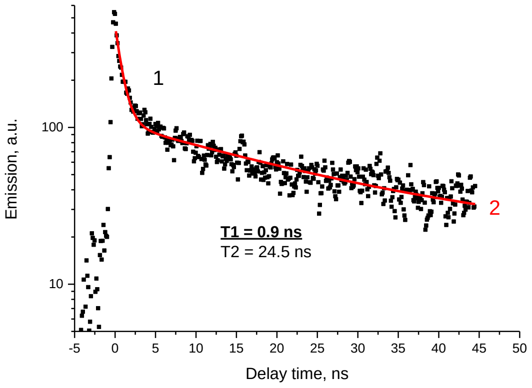

Figure S26. Time-resolved decay of emission of hybrid material **8**-In_2O_3 (λ_{exc} = 460 nm, emission range: 560-620 nm, 1, black) in the air, and the best biexponential fit of luminescence decay (2, red) in log scale. T1, T2 – luminescence lifetimes.

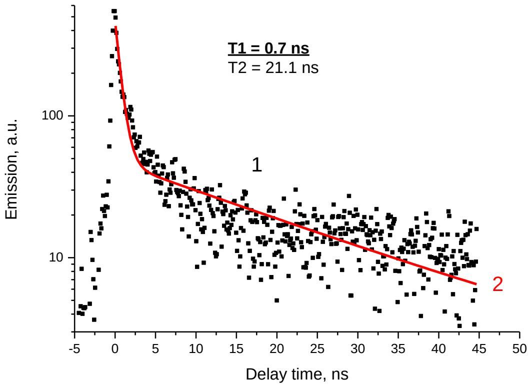

Figure S27. Time-resolved decay of emission of hybrid material **8**-SnO_2 (λ_{exc} = 460 nm, emission range: 560-620 nm, 1, black) in the air, and the best biexponential fit of luminescence decay (2, red) in log scale. T1, T2 – luminescence lifetimes.

Electrochemistry studies

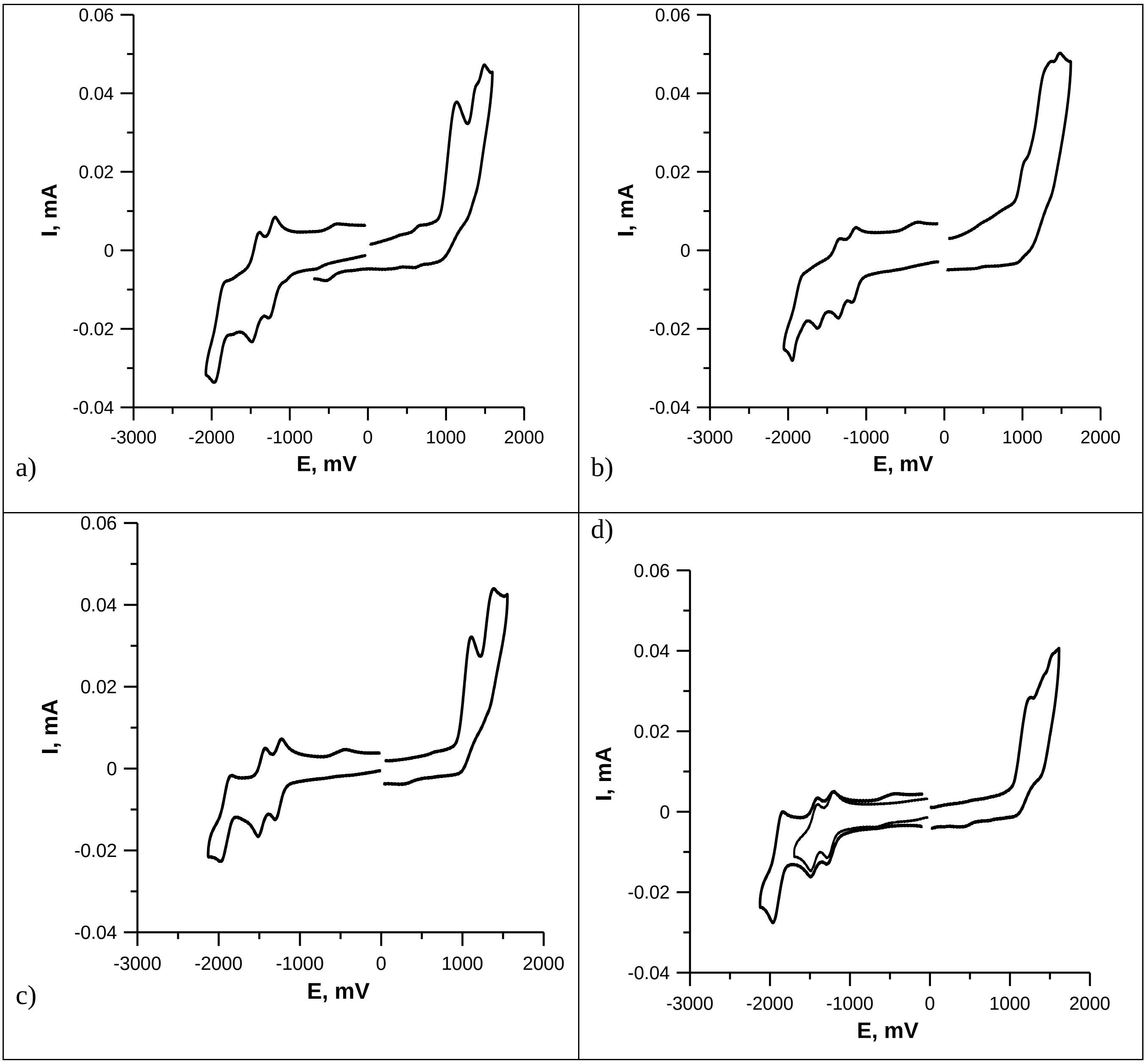

Figure S28. Cyclic voltammograms of **5** (a), **6** (b), **7** (c), **8** (d), obtained on GC electrode

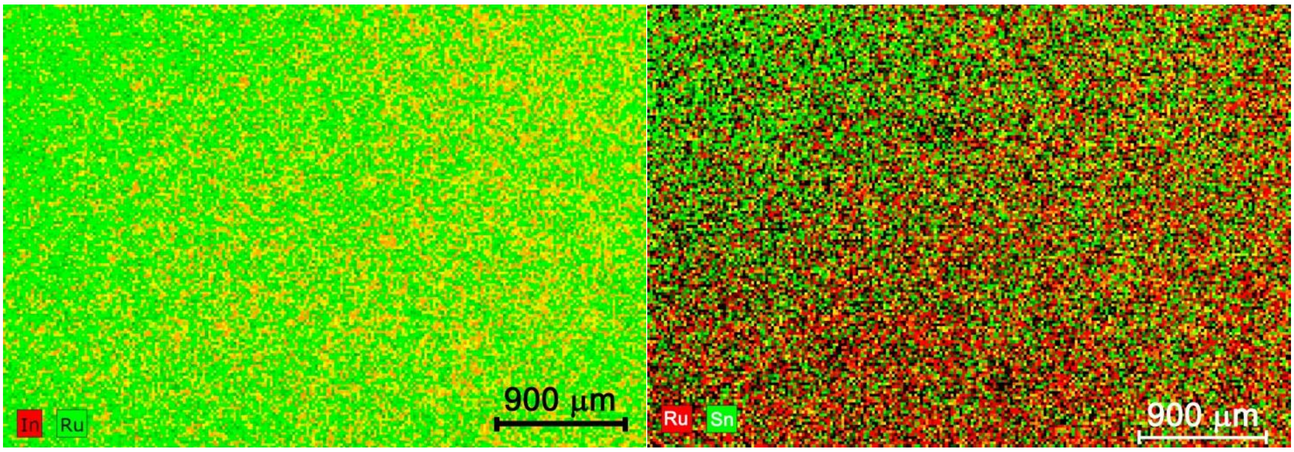

Figure S29. X-ray fluorescence maps of the distribution of elements on the surface of hybrid materials based on complex **8** and semiconductor oxides In_2O_3 (left) and SnO_2 (right) nanoparticles.

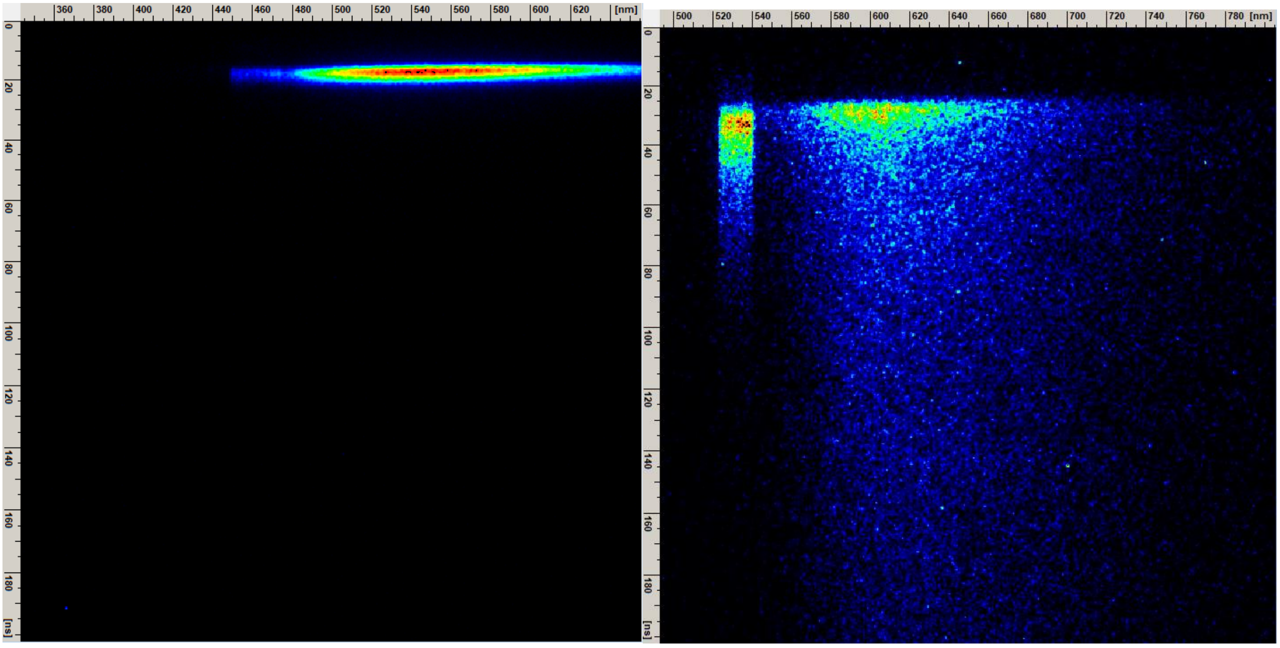

Figure S30. Luminescence decay maps for unmodified SnO_2 nanoparticles (left) and hybrid material **5**-SnO_2

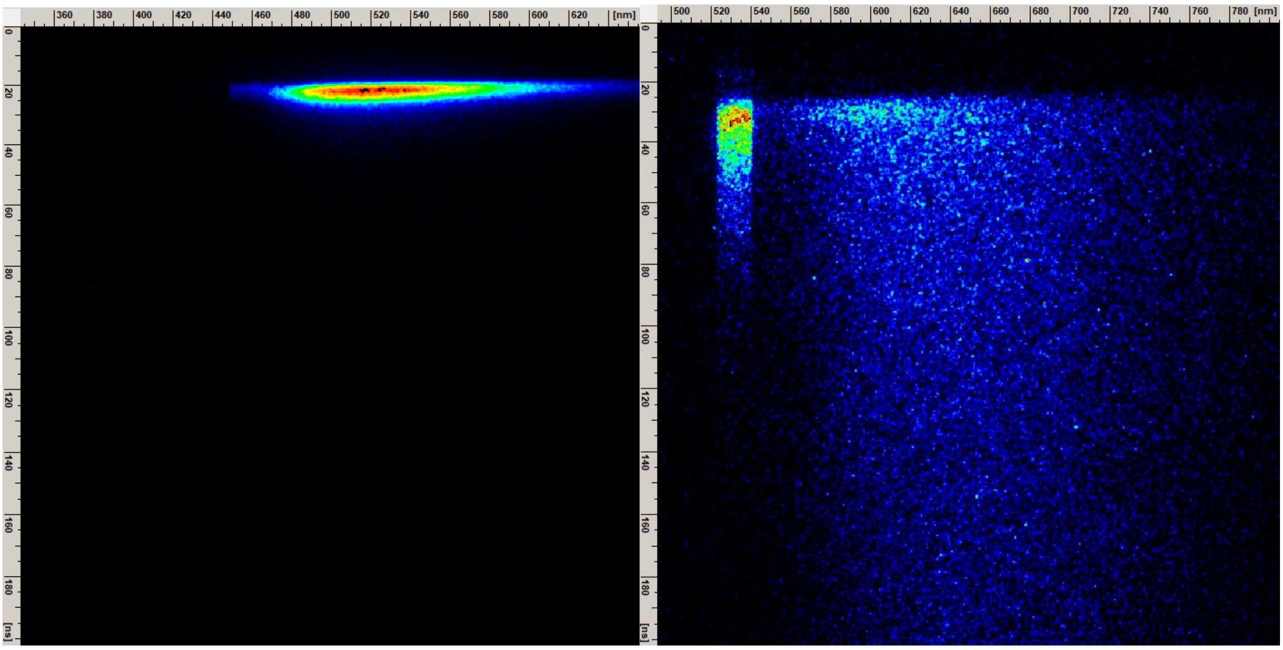

Figure S31. Luminescence decay maps for unmodified In_2O_3 nanoparticles (left) and hybrid material **5**- In_2O_3

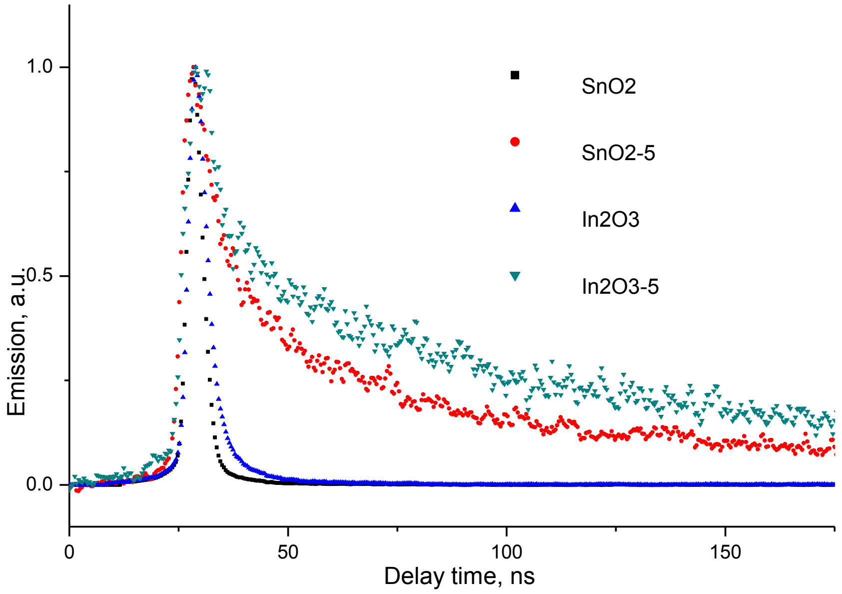

Figure S32. Time-resolved emission decays of unmodified semiconductors and hybrid materials (λ_{exc} = 460 nm, emission range: 560-620 nm), obtained from luminescence decay maps S30, S31. Curves were normalized and shifted for their maxima to overlay.

References:

1. R.H. Zheng, H.C. Guo, H.J. Jiang, K.H. Xu, B.B. Liu, W.L. Sun, Z. Q. Shen, A new and convenient synthesis of phendiones oxidated by $KBrO_3/H_2SO_4$ at room temperature, Chinese Chemical Letters 2010 V. 21, № 11, P. 1270-1272
2. Zhang X., Li L.L., Liu Y. Fluorescent detection and imaging of Hg^{2+} using a novel phenanthroline derivative based single- and two-photon excitation // Mater. Sci. Eng., C. 2016. V. 59. P. 916-923
3. Day A. R., Steck E. A. Reactions of phenanthraquinone and retenequinone with aldehydes and ammonium acetate in acetic acid solution. // J. Am. Chem. Soc. 1943.V. 65. P. 452-456.
4. Batista R.M.F., Costa S.P.G., Belsley M., Lodeiro C., Raposo M.M.M. Synthesis and characterization of novel (oligo)thienyl-imidazo-phenanthrolines as versatile p-conjugated systems for several optical applications. // Tetrahedron. 2008. V. 64. № 39. P. 9230-9238
5. J.-Z. Wu, B.-H. Ye, L. Wang, L.-N. Ji, J.-Y. Zhou, R.-H. Li, Z.-Y. Zhouc. Bis(2,2-bipyridine)ruthenium(II) complexes with imidazo[4,5-f][1,10]- phenanthroline or 2-phenylimidazo[4,5-f][1,10]phenanthroline. // J. Chem. Soc., Dalton Trans. (1997) 1395
6. J. Bingwen , W. Tao , T. Chunhong , Z. Manhua , S. Tao. pH-Dependent luminescence of ruthenium(II) polypyridine complexes // Bull. Chem. Soc. Japan. 73 (2000) 1749
7. Li Z., Yang H., Zhang A., Luo H., Wanga K. pH effects on optical and DNA binding properties of a thiophene-containing ruthenium(II) complex. // Inorg. Chim. Acta. 2011. V. 370. P. 132-140.
8. J.-Z. Wu, B.-H. Ye, L. Wang, L.-N. Ji, J.-Y. Zhou, R.-H. Li, Z.-Y. Zhouc. Bis(2,2-bipyridine)ruthenium(II) complexes with imidazo[4,5-f][1,10]- phenanthroline or 2-phenylimidazo[4,5-f][1,10]phenanthroline. // J. Chem. Soc., Dalton Trans. (1997) 1395
9. M.R. Reddy, P.V. Reddy, Y.P. Kumar, A. Shrishailam, N. Nambigari, S. Satyanarayana. Synthesis, characterization , DNA binding, light switch «on and off», docking studies and cytotoxicity of ruthenium (II) and cobalt (III) polypyridil complexes // J. Fluoresc. 24 (2014) 803-817

10. Z.-S. Li, H.-X. Yang, A.-G. Zhang, H. Luo, K.-Z. Wang. pH effects on optical and DNA binding properties of athiophene-containing ruthenium (II) complex // Inorganica Chimica Acta 370 (2011) 132-140

11. Chizhov, A.; Rumyantseva, M.; Vasiliev, R.; Filatova, D.; Drozdov, K.; Krylov, I.; Marchevsky, A.; Karakulina, O.; Abakumov, A.; Gaskov, A. Visible light activation of room temperature NO2 gas sensors based on ZnO, SnO2 and In2O3 sensitized with CdSe quantum dots. Thin Solid Films 2016, 618, 253–262